19th Australasian Fluid Mechanics Conference
Melbourne, Australia
8-11 December 2014

Unsteady Turbulence in a Tidal Bore: Field Measurements in the Garonne River in October 2013

H. Chanson[1], D. Reungoat[2] and C. Keevil[3]

[1]School of Civil Engineering
University of Queensland, Brisbane QLD 4072, Australia

[2]I2M - Laboratoire TREFLE
University of Bordeaux, Pessac, France

[3]Department of Geography, Environment and Earth Sciences
University of Hull, Hull HU6 7RX, United Kingdom

Abstract

A tidal bore is an unsteady rapidly-varied free-surface flow generated by the rapid rise in water elevation during the early flood tide, when the tidal range exceeds 4.5 to 6 m and the channel bathymetry amplifies the flood tidal wave. This study describes a detailed field investigation conducted in the Garonne River (France). The tidal bore was undular on 19 October 2013 and the bore front was followed by some well-defined whelps. The instantaneous velocity data indicated large and rapid fluctuations of all velocity components during the tidal bore. Large Reynolds shear stresses were observed during and after the tidal bore passage. Altogether the investigation characterised some unusual turbulence transient in a large river system.

Introduction

A tidal bore is a series of waves propagating upstream in an estuarine zone, when the tidal flow turns to rising (Fig. 1). It is an unsteady rapidly-varied free-surface flow generated by the rapid rise in water elevation during the early flood tide, when the tidal range exceeds 4.5 to 6 m and the channel bathymetry amplifies the flood tidal wave (Tricker 1965, Lighthill 1978). The existence of the tidal bore is based upon a delicate balance between the tidal amplitude, the freshwater river flow conditions and the estuarine channel bathymetry. This balance may be easily disturbed by changes in boundary conditions and freshwater runoff, and a number of man-made interventions led to the modification and sometimes disappearance of tidal bores, for example in France, Canada, Mexico (Chanson 2011). A related process is the tsunami-induced bore. When a tsunami wave propagates upriver, its leading edge may be led by a positive surge (Tanaka et al. 2012). The tsunami-induced bore may propagate into the rivers far upstream, as seen in Japan in 1983, 2001, 2003 and 2011, during the 26 December 2004 tsunami disaster in the Indian Ocean, and in the River Yealm in United Kingdom on 27 June 2011.

The inception and development of a tidal bore may be predicted using the shallow-water equations. After formation, the bore front may be analysed as a hydraulic jump in translation (Lighthill 1978, Liggett 1994). Neglecting the boundary friction, the equations of conservation of mass and momentum in their integral form give a relationship between the ratio of conjugate cross-section areas A_2/A_1 and the tidal bore Froude number Fr_1 for a flat horizontal channel (Chanson 2012):

$$\frac{A_2}{A_1} = \frac{1}{2} \times \frac{\sqrt{\left(2 - \frac{B'}{B}\right)^2 + 8\frac{\frac{B'}{B}}{\frac{B_1}{B}} \times Fr_1^2} - \left(2 - \frac{B'}{B}\right)}{\frac{B'}{B}} \quad (1)$$

where the Froude number is defined as:

$$Fr_1 = \frac{V_1 + U}{\sqrt{g \times \frac{A_1}{B_1}}} \quad (2)$$

V_1 is the initial river flow velocity positive downstream, U is the bore celerity positive upstream, g is the gravity acceleration, B_1 is the initial free-surface width, and B and B' are the characteristic free-surface widths (Chanson 2012)

In the present study, new field measurements were conducted in the tidal bore of the Garonne River (France) on 19 October 2013. The turbulent velocity measurements were performed continuously at high frequency (200 Hz) prior to, during and after the tidal bore. It is the aim of this contribution to characterise simultaneously the unsteady water elevation and velocity field, including the Reynolds stresses.

Figure 1. Tidal bore of the Garonne River (France) - Top: Arcins on 19 October 2013 (Courtesy of Ludovic Osmar) - Bottom: Podensac on 23 August 2013, 26 km upstream of Arcins.

Field Study and Instrumentation

The field study was conducted in the Arcins channel of the Garonne River (France), between the Arcins Island and the right bank, about 6.5 km south-west of the centre of the City of Bordeaux. The Arcins channel is about 1.8 km long, 70 m wide and about 1.1 to 2.5 m deep at low tide (Fig. 2). Figure 1 Top shows the Arcins channel and Figure 2 presents a cross-sectional survey conducted on 19 October 2013, with z being the vertical elevation in m NGF IGN69. The field measurements were conducted under spring tide conditions on 19 October 2013 afternoon, at the same site as Chanson et al. (2011) and Reungoat et al. (2014). The tidal range was 6.09 m on 19 October 2013 and the tidal cycles in Bordeaux had slightly different periods and amplitudes typical of some diurnal inequality. The field measurements were conducted prior to, during and after the passage of the tidal bore in the afternoon. Further information on the field measurements and data were reported in Reungoat et al. (2014).

The free surface elevations were measured manually using a survey staff. During the passage of the tidal bore, a video camera recorded the water level at 25 fps. The survey staff was mounted about 2 m from the ADV unit towards the right bank, to minimise any interference with the ADV sampling volume. The instantaneous velocity components were measured with a Nortek^{TM} ADV Vectrino+ (10 MHz, serial number VNO1356). The ADV system was equipped with a down-looking head (ADV field) equipped with four receivers. The ADV unit was fixed beneath a hull of a heavy and sturdy pontoon and mounted vertically. Figure 2 shows the location of the ADV sampling volume in the surveyed cross-section at low tide. For the study, the velocity range was 2.5 m/s, the ADV was set up with a transmit length of 0.3 mm and a sampling volume of 1.5 mm height. The ADV system was sampled continuously at 200 Hz, between 3 h before and 90 min after the tidal bore. The ADV data underwent a post-processing procedure to eliminate any erroneous or corrupted data from the data sets to be analysed. The post processing was conducted with the software WinADV^{TM} version 2.028. It included the removal of communication errors, the removal of average signal to noise ratio (SNR) data less than 5 dB, the removal of average correlation values less than 60% following McLelland and Nicholas (2000) and despiking using the phase-space thresholding technique developed by Goring and Nikora (2002). The percentage of good samples was superior to 82% for the entire data set.
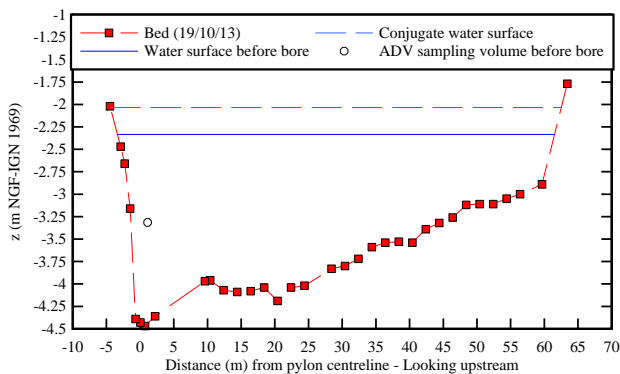
Figure 2. Surveyed (distorted) cross-section of the Arcins channel at the sampling location, looking upstream (i.e. South) - Water levels immediately before and after bore front are shown (19 October 2013).

Basic Observations

The tidal bore formed at the northern end of the channel and extended across the entire channel width (Fig. 1 Top). As the bore propagated upstream, its shape evolved in response to the local bathymetry. The tidal bore was undular when it passed the sampling location. The bore front was well highlighted by the surfers riding ahead of the first wave crest (Fig. 1). The bore passage was followed by a series of whelps lasting for a couple of minutes, with a wave period of about 1 s. The free-surface elevation rose very rapidly by 0.3 m in the first 10-15 s (Fig. 3, star symbols). For the next 60 s, the water elevation rose further by 1.1 m.

The tidal bore front was characterised by a marked rise in free-surface elevation. The Froude number was calculated based upon the surveyed channel cross-section and field observations yielding $Fr_1 = 1.27$. Such a Froude number was consistent with the undular nature of the bore. The present observations are reported in Figure 4 in terms of the ratio of conjugate cross-sectional areas A_2/A_1 as a function of the Froude number Fr_1. The present data (red star symbol) are compared with the momentum principle solution (Eq. (1)) (open circles) and previous field data (solid blue symbols) (Fig. 4). For completeness, the Bélanger equation developed for a smooth rectangular channel is included:

$$\frac{A_2}{A_1} = \frac{1}{2} \times \left(\sqrt{1 + 8 \times Fr_1{}^2} - 1 \right) \qquad (3)$$

Figure 4 presents a good agreement between Equation (1) and the field data, indicating further the limitations of the Bélanger equation (Eq. (3)) in natural estuarine channels.
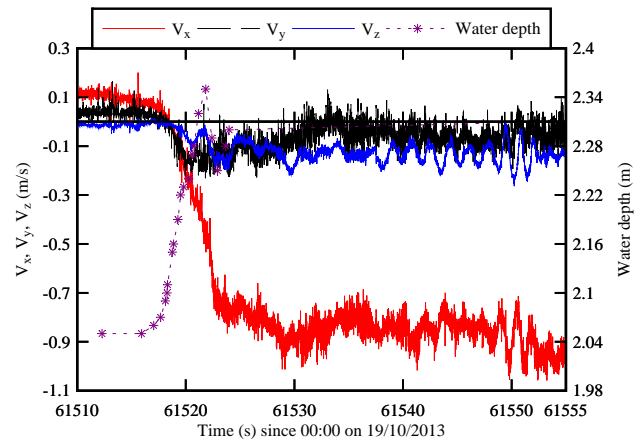
Figure 3. Water depth and instantaneous velocity components as functions of time during the tidal bore passage.
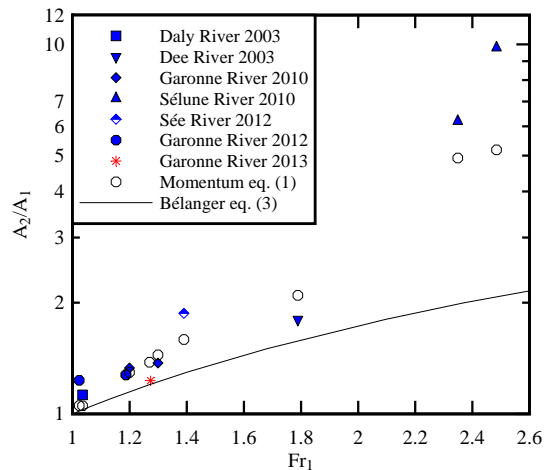
Figure 4. Relationship between the conjugate cross-sectional area ratio A_2/A_1 and Froude number Fr_1 - Comparison between field observations, momentum equation (Eq. (1)) and the Bélanger equation (Eq, (3)).

Free-surface properties

The passage of the undular bore was associated with a rapid rise in water elevation (t = 61,512 s in Fig. 3) and some pseudo-chaotic wave motion afterwards. A key feature of the bore was the smooth front followed by a secondary wave motion. Such a feature was previously documented during field experiments (Wolanski et al. 2004, Chanson et al. 2011). The dimensionless wave steepness and wave length data are presented in Figure 5. In Figure 5, the present observations are compared to field and laboratory data as well as to analytical solutions. The undular bore data indicated an increase in wave steepness a_w/L_w with increasing Froude number up to $Fr_1 = 1.3$ to 1.35 (Fig. 5A). It is believed that the maximum steepness was restricted by the appearance of some breaking at the first wave crest. For larger Froude numbers, the wave steepness data tended to decrease with increasing Froude number. The dimensionless wave length $L_w/(A_1/B_1)$ decreased with increasing Froude number and the data were relatively close to a solution of the Boussinesq equation (Fig. 5B). The present data (red star symbol) showed comparable data trends with previous field and laboratory observations, despite the irregular bathymetry of the natural estuaries.
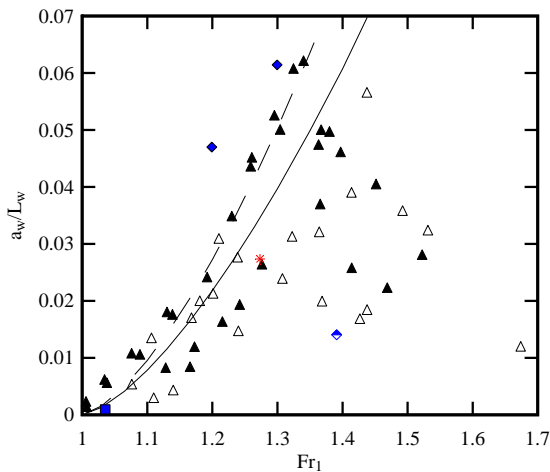
(A)
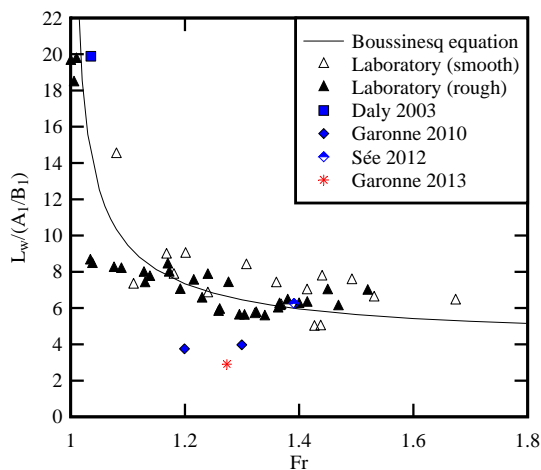
(B)

Figure 5. Wave steepness and dimensionless wave length of prototype undular bores - Comparison with laboratory data, linear wave theory (dashed line) and Boussinesq equation solution (solid line)- Same legend for both graphs.

Velocity and Turbulent Stress Data

Velocity Measurements

The instantaneous velocity components were measured prior to, during and after the tidal bore. Figure 3 shows the data about the time of passage of the bore front, with the longitudinal velocity component V_x positive downstream towards Bordeaux, the transverse velocity component V_y positive towards the Arcins Island, and the vertical velocity component V positive upwards. The time-variations of the water depth are also included (Fig. 3).

For the last two hours prior to the tidal bore, the ebb tide current velocity dropped from +0.6 m/s down to +0.1 m/s. The tidal bore passage (t = 61,512 s) induced a marked effect on the velocity field (Fig. 3). The main current reversed its direction almost immediately and the mean longitudinal velocity ranged typically between -0.8 and -1.2 m/s after the bore passage, where the negative sign reflected the upriver flow direction. During the bore passage, the maximum longitudinal flow deceleration was -0.18 m/s², or -0.02×g. The tidal bore passage was characterised by large fluctuations of all velocity components. The longitudinal velocity component fluctuated between -0.6 to -1.35 m/s after the passage of the bore, the transverse velocities ranged from -0.2 to +0.35 m/s, while the vertical velocity data fluctuated between -0.3 and +0.1 m/s.

The vertical velocity data showed some oscillations with period about 1 to 1.5 s immediately after the bore passage (61,520 < t < 61,555 s, Fig. 3). It is believed that these oscillations were closely linked with the free-surface undulations, or whelps, and their induced vertical motion. The irrotational flow theory predicts a redistribution of both longitudinal and vertical velocities beneath undulations between wave crests and troughs, with the same periodicity as the free-surface elevation but out of phase (Rouse 1938, Montes and Chanson 1998). This pattern would be consistent with the present observations and it was previously documented experimentally in laboratory tidal bores (Koch and Chanson 2008, Chanson 2010).

Turbulent Reynolds stresses

A Reynolds stress is proportional to the cross-product of turbulent velocity fluctuation v, where v is the deviation of the instantaneous velocity V from a 'mean' value. Herein the 'mean value' was the variable interval time average VITA calculated using a threshold frequency of 2 Hz (Chanson and Docherty 2012). The filtering was applied to all velocity components and the turbulent Reynolds stresses were calculated from the high-pass filtered signals. Typical results are presented in Figure 6.

The field observations showed large turbulent shear stresses and large and rapid fluctuations in shear stresses during and after the tidal bore, for all Reynolds stress tensor components. Overall the measurements indicated that the turbulent shear stresses were significantly larger after the tidal bore passage (Fig. 6). Maximum instantaneous shear stress amplitudes of up to 80 Pa were recorded during and after the tidal bore. The data indicated that the tidal bore likely scoured the channel bed and advected into suspension the bed material and 'washload' upstream, behind the bore front during the early flood tide. The process applied to a significant length of the estuarine section of the Garonne River and would mobilise an enormous amount of sediments.

(A) $\rho \times v_x^2$ and $\rho \times v_x \times v_y$

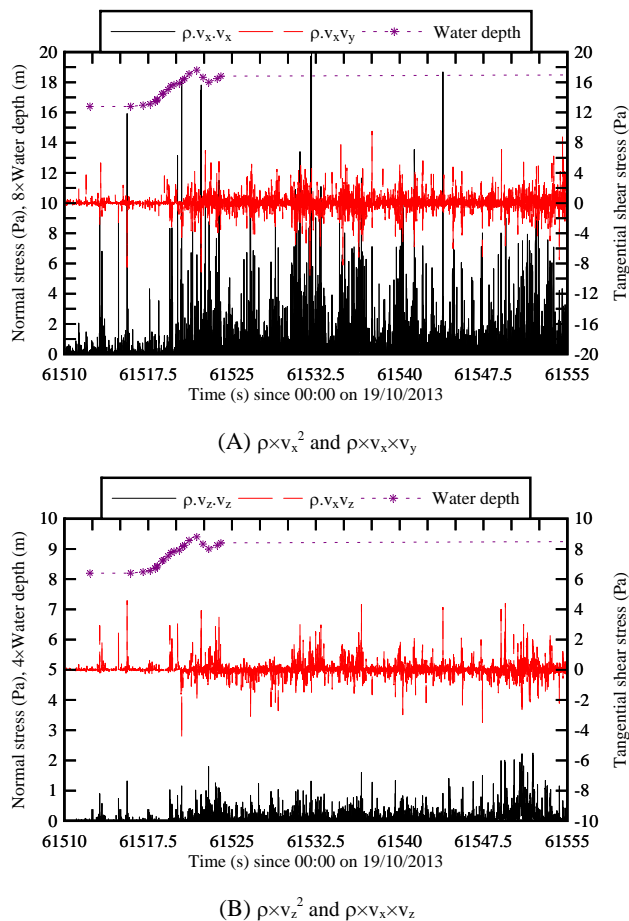(B) $\rho \times v_z^2$ and $\rho \times v_x \times v_z$

Figure 6. Time-variations of Reynolds stresses during the bore passage.

Conclusion

During a field study in the Garonne Rive (France), the turbulent mixing induced by a tidal bore was documented with a fine temporal resolution (200 Hz). The tidal bore was undular and its Froude number was $Fr_1 = 1.27$. The undular bore front was followed by some well-defined whelps with wave period about 1 s and wave amplitude and length comparable to theoretical estimates.

The instantaneous velocity data indicated large and rapid fluctuations of all velocity components. Large Reynolds shear stresses were observed during and after the tidal bore. The amplitude of the instantaneous turbulent shear stresses was one to two orders of magnitude larger than the critical stress for sediment motion onset, thus explaining the very turbid waters observed after the bore.

Acknowledgments

References

[1] Chanson, H. (2010). Unsteady Turbulence in Tidal Bores: Effects of Bed Roughness. *Journal of Waterway, Port, Coastal, and Ocean Engineering*, ASCE, Vol. 136, No. 5, pp. 247-256 (DOI: 10.1061/(ASCE)WW.1943-5460.0000048).

[2] Chanson, H. (2011). Tidal Bores, Aegir, Eagre, Mascaret, Pororoca: Theory and Observations. *World Scientific*, Singapore, 220 pages.

[3] Chanson, H. (2012). Momentum Considerations in Hydraulic Jumps and Bores. *Journal of Irrigation and Drainage Engineering*, ASCE, Vol. 138, No. 4, pp. 382-385 (DOI 10.1061/(ASCE)IR.1943-4774.0000409).

[4] Chanson, H., and Docherty, N.J. (2012). Turbulent Velocity Measurements in Open Channel Bores. *European Journal of Mechanics B/Fluids*, Vol. 32, pp. 52-58 (DOI 10.1016/j.euromechflu.2011.10.001).

[5] Chanson, H., Reungoat, D., Simon, B., and Lubin, P. (2011). High-Frequency Turbulence and Suspended Sediment Concentration Measurements in the Garonne River Tidal Bore. *Estuarine Coastal and Shelf Science*, Vol. 95, No. 2-3, pp. 298-306 (DOI 10.1016/j.ecss.2011.09.012).

[6] Goring, D.G., and Nikora, V.I. (2002). Despiking Acoustic Doppler Velocimeter Data. *Journal of Hydraulic Engineering*, ASCE, Vol. 128, No. 1, pp. 117-126.

[7] Liggett, J.A. (1994). Fluid Mechanics. *McGraw-Hill*, New York, USA.

[8] Lighthill, J. (1978). Waves in Fluids. *Cambridge University Press*, Cambridge, UK, 504 pages.

[9] McLelland, S.J., and Nicholas, A.P. (2000). A New Method for Evaluating Errors in High-Frequency ADV Measurements. *Hydrological Processes*, Vol. 14, pp. 351-366.

[10] Montes, J.S., and Chanson, H. (1998). Characteristics of Undular Hydraulic Jumps. Results and Calculations. *Journal of Hydraulic Engineering*, ASCE, Vol. 124, No. 2, pp. 192-205.

[11] Reungoat, D., Chanson, H., and Caplain, B. (2014). Sediment Processes and Flow Reversal in the Undular Tidal Bore of the Garonne River (France). *Environmental Fluid Mechanics*, Vol. 14, No. 3, pp. 591–616 (DOI: 10.1007/s10652-013-9319-y).

[12] Reungoat, D., Chanson, H., and Keevil, C. (2014). Turbulence, Sedimentary Processes and Tidal Bore Collision in the Arcins Channel, Garonne River (October 2013). *Hydraulic Model Report No. CH94/14*, School of Civil Engineering, The University of Queensland, Brisbane, Australia, 145 pages.

[13] Rouse, H. (1938). Fluid Mechanics for Hydraulic Engineers. *McGraw-Hill Publ.*, New York, USA.

[14] Tanaka, H., Nguyen, X.T., Umeda, M., Hirao, R., Pradjoko, E., Mano, A., and Udo, K. (2012). Coastal and Estuarine Morphology Changes Induced by the 2011 Great East Japan Earthquake Tsunami. *Coastal Engineering Journal*, Vol. 54, No. 1, paper 1250010, 25 pages (DOI: 10.1142/S0578563412500106).

[15] Tricker, R.A.R. (1965). Bores, Breakers, Waves and Wakes. *American Elsevier Publ. Co.*, New York, USA.

[16] Wolanski, E., Willimas, D., Spagnol, S., and Chanson, H. (2004). Undular Tidal Bore Dynamics in the Daly Estuary, Northern Australia. *Estuarine, Coastal and Shelf Science*, Vol. 60, No. 4, pp. 629-636.